Magnetic and orbital orders coupled to negative thermal expansion in Mott insulators Ca$_2$Ru$_{1-x}M_x$O$_4$ (M = Mn and Fe)

T. F. Qi,[1,2] O. B. Korneta,[1,2] S. Parkin,[1,3] Jiangping Hu,[4] and G. Cao[1,2,*]

[1]*Center for Advanced Materials, University of Kentucky, Lexington, Kentucky 40506, USA*

[2]*Department of Physics and Astronomy, University of Kentucky, Lexington, Kentucky 40506, USA*

[3]*Department of Chemistry, University of Kentucky, Lexington, Kentucky 40506, USA*

[4]*Department of Physics, Purdue University, West Lafayette, Indiana 47907, USA*

Ca$_2$RuO$_4$ is a structurally driven Mott insulator with a metal-insulator transition at $T_{MI} = 357$K, followed by a well-separated antiferromagnetic order at $T_N = 110$ K. Slightly substituting Ru with a 3d transition metal ion M effectively shifts T_{MI} by weakening the orthorhombic distortion and induces either metamagnetism or magnetization reversal below T_N. Moreover, M doping for Ru produces negative thermal expansion in Ca$_2$Ru$_{1-x}M_x$O$_4$ (M = Cr, Mn, Fe, or Cu); the lattice volume expands on cooling with a total volume expansion ratio, $\Delta V/V$, reaching as high as 1%. The onset of the negative thermal expansion closely tracks T_{MI} and T_N, sharply contrasting classic negative thermal expansion that shows no relevance to electronic properties. In addition, the observed negative thermal expansion occurs near room temperature and extends over a wide temperature interval up to 300 K. These findings underscore new physics driven by a complex interplay between orbital, spin, and lattice degrees of freedom.

I. INTRODUCTION

The Coulomb interaction U is generally comparable to the 4d-bandwidth W in the 4d-based ruthenates, A$_{n+1}$Ru$_n$O$_{3n+1}$ with $n = 1, 2, 3, \infty$ (A = Ca or Sr), which leaves them precariously balanced on the border between metallic and insulating behavior and/or on the verge of long-range magnetic order. A common characteristic of these materials is that underlying physical properties are critically linked to the lattice and orbital degrees of freedom and tend to exhibit a nonlinear or giant response to modest lattice changes. This is illustrated by observations of a p-wave superconducting state in Sr$_2$RuO$_4$[1] and a first-order metal-insulator (MI) transition at $T_{MI} = 357$ K, which is followed by a well-separated antiferromagnetic transition at $T_N = 110$ K in Ca$_2$RuO$_4$ that is more structurally distorted due to the smaller ionic radius $r_{Ca} < r_{Sr}$.[2,3]

In Ca$_2$RuO$_4$, the MI transition induces a radical change in electrical resistivity $\rho(T)$ by over nine orders of magnitude below T_{MI}, which also marks a concomitant and violent structural transition between a high-T tetragonal and a low-T orthorhombic phase at T_{MI} or a strong cooperative Jahn-Teller distortion.[2–4] Below T_{MI}, the a axis contracts by 1.5%, but the b axis expands by 3% on cooling, over a temperature interval of 250 K; the combined effect of these conflicting uniaxial thermal expansions is to drive an increasingly strong orthorhombic distortion in the basal plane that shatters single-crystal samples and contracts the lattice volume by 1.3% as temperature is lowered from 400 K to 70 K.[2,3] It is already established that such a strong cooperative Jahn-Teller distortion removes the degeneracy of the three Ru t_{2g} orbitals (d_{xy}, d_{yz}, d_{zx}) via a transition to orbital order that, in turn, drives the MI transition at $T_{MI} = 357$ K,[5–9] which is followed by an antiferromagnetic order at $T_N = 110$ K that is well below $T_{MI} = 357$ K, sharply contrasting classic Mott insulators that undergo simultaneous transitions to antiferromagnetic order and an insulating state at T_{MI}. This behavior, which is also observed in its sister compound, Ca$_3$Ru$_2$O$_7$,[10] separates the layered Ca$_{n+1}$Ru$_n$O$_{3n+1}$ ($n = 1$ and 2) from classic Mott insulators as a unique archetype of Mott insulators in which the MI transition is not primarily driven by antiferromagnetic order. Controversy over the exact nature of the orbital state remains, but the extraordinary sensitivity of T_{MI} to modest changes in lattice parameters or modest pressure[5–9,11–13] clearly indicate that the lattice and orbital degrees of freedom play a decisive role in the new physics that drives Ca$_2$RuO$_4$.

Indeed, we have recently observed that modest Cr doping for Ru in Ca$_2$RuO$_4$ not only changes T_{MI} and the magnetic behavior below T_N but also triggers off a two-step, abrupt negative thermal expansion (NTE) at T_{MI} and T_N and a nearly zero thermal expansion between T_C and T_{MI}, giving rise to a total volume expansion ratio $\Delta V/V \approx 1\%$ on cooling over $90 < T < 220$ K. This behavior indicates that the observed NTE is strongly coupled to the orbital and magnetic orders,[14] in contrast to classic NTE primarily driven by phonon modes or geometry effects.[15–21] The observed lattice anomaly at T_N is clearly a magnetovolume effect, which originates from a strong correlation between the lattice expansion and spin frustration.[14] It is noted that the origin of the NTE recently observed in BiNiO$_3$ is attributed to charge transfer.[22]

In this paper we report results of our more recent study that we have extended to include other 3d ion dopants. The central findings of this study are that the strong coupling of the NTE to orbital and magnetic orders is in fact a common occurrence in a class of materials, Ca$_2$Ru$_{1-x}M_x$O$_4$, where M = Mn, Fe, or Cu, and that M doping effectively changes T_{MI} by weakening the orthorhombic distortion and induces unusual magnetic behavior such as metamagneticsm and magnetization reversal below T_N. In the following we present and discuss the underlying physical properties and the NTE observed in Mn- and Fe-doped Ca$_2$RuO$_4$. The simultaneous occurrence of the NTE and orbital and magnetic orders underscores a mechanism driven by complex electronic correlations; this mechanism is qualitatively discussed.

II. EXPERIMENTAL TECHNIQUES AND STRUCTURAL REFINEMENTS

The single crystals of $Ca_2Ru_{1-x}M_xO_4$, with $M =$ Mn and Fe and $0 \leqslant x \leqslant 0.25$, were grown using a floating-zone optical furnace; details of single-crystal growth are described elsewhere.[14,23] Our single-crystal x-ray diffraction study of $Ca_2Ru_{1-x}M_xO_4$ was performed as a function of temperature between 90 K and 430 K using a Nonius-Kappa CCD single-crystal x-ray diffractometer. The structures were refined by the SHELX-97 programs.[24,25] All structures affected by absorption and extinction were corrected by comparison of symmetry-equivalent reflections using the program SADABS.[25] It needs to be emphasized that the single crystals are of high quality and there is no indication of any mixed phases or inhomogeneity in all doped single crystals studied. The presence of any mixed phases or inhomogeneity in the single crystals would not allow any converging structural refinements. Some of the experimental and refinement details for three different dopants at a similar doping concentration are given in Table I. (The data Cr doping is also listed for the purpose of comparison.) Single crystal diffraction data collected from $Ca_2Ru_{1-x}M_xO_4$ samples are indexed on the basis of the orthorhombic symmetry shown in Table II. Note that errors of the last digit given in parentheses represent only statistical errors, not systematic errors, which may arise from correlations between parameters. The rest of the structure data including x and temperature dependence will be published

elsewhere.[26] Error bars for the structural data presented here are smaller than the symbols, therefore are not included. It is noted that the value of the R-factor ($= 0.067$) for the Mn-doped crystal is greater that those for other two samples but still well within the range for good-quality refinements. The reason that the values of R and wR (weighted R factor) for this sample are larger is because the crystal used for this particular diffraction measurement is significantly smaller than those of the other two (see Table I); this results in a set of weaker diffraction peaks, thus larger wR, which is based on intensities. Chemical compositions were determined by both energy dispersive x-ray (EDX) and single-crystal x-ray diffraction; the two probes always yield consistent values for chemical compositions. (The EDX analysis was performed using a brand new set of Hitachi/Oxford SEM/EDX.) The EDX data also confirmed the high homogeneity of all crystals studied. Measurements of magnetization $M(T, H)$, heat capacity $C(T)$, and electrical resistivity $\rho(T)$ for $1.7 < T < 400$ K were performed using either a Quantum Design Physical Property Measurement System or Magnetic Property Measurement System.

III. RESULTS AND DISCUSSIONS

A. $Ca_2Ru_{1-x}Mn_xO_4$ with $0 < x \leqslant 0.25$

Figure 1(a) exhibits the lattice parameters for the a, b, and c axes at $T = 90$ K as a function of Mn concentration x ranging from 0 to 0.25 for single-crystal $Ca_2Ru_{1-x}Mn_xO_4$.

TABLE I. Experimental and refinement details of $Ca_2Ru_{1-x}M_xO_4$ ($M =$ Cr, Mn, and Fe).

	$Ca_2Ru_{1-x}\mathbf{Cr}_xO_4$	$Ca_2Ru_{1-x}\mathbf{Mn}_xO_4$	$Ca_2Ru_{1-x}\mathbf{Fe}_xO_4$
Crystal data			
Chemical formula	$Ca_4Ru_{1.87}$ $Cr_{0.13}O_8$	$Ca_4Ru_{1.9}$ $Mn_{0.1}O_8$	$Ca_4Ru_{1.88}$ $Fe_{0.12}O_8$
M_r	474.02	490.46	490.46
Crystal system, space group	Orthorhombic, *Pbca*	Orthorhombic, *Pbca*	Orthorhombic, *Pbca*
Temperature (K)	90 K	90 K	90 K
a, b, c (Å)	5.3917 (2), 5.5157 (2), 11.8804 (4)	5.3856 (1), 5.5875 (2), 11.7772 (4)	5.4045 (1), 5.5809 (2), 11.7718 (6)
α, β, γ (°)	90, 90, 90	90, 90, 90	90, 90, 90
V (Å^3)	353.31 (2)	354.40 (2)	355.06 (2)
Z	2	2	2
Radiation type	Mo $K\alpha$	Mo $K\alpha$	Mo $K\alpha$
μ (mm^{-1})	6.99	7.17	7.15
Crystal size (mm)	$0.05 \times 0.05 \times 0.05$	$0.01 \times 0.05 \times 0.05$	$0.01 \times 0.1 \times 0.03$
Data collection			
Diffractometer	Nonius KappaCCD diffractometer	Nonius KappaCCD diffractometer	Nonius KappaCCD diffractometer
Absorption correction	Multiscan SADABS(Sheldrick, 1996)	Multiscan SADABS(Sheldrick, 1996)	Multiscan SADABS(Sheldrick, 1996)
No. of measured, independent and observed[$I > 2\sigma(I)$] reflections	7241, 398, 352	4888, 350, 294	4924, 398, 289
R_{int}	0.030	0.055	0.046
Refinement			
$R[F^2 > 2\sigma(F^2)]$, $wR(F^2)$, S	0.016, 0.046, 1.13	0.067, 0.173, 1.30	0.032, 0.089, 1.14
No. of reflections	398	350	398
No. of parameters	36	35	36
No. of restraints	0	0	0
$\Delta\rho_{max}$, $\Delta\rho_{min}$ (e Å^{-3})	0.66, -0.60	2.99, -2.90	2.05, -1.35
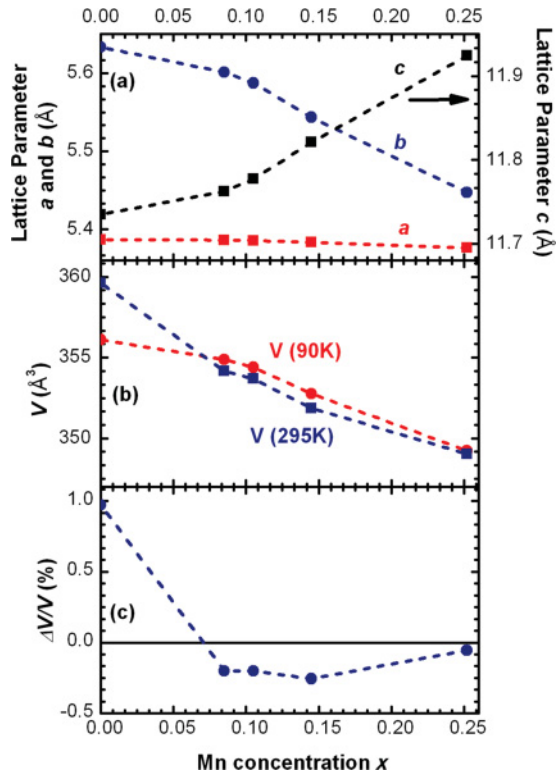
FIG. 1. (Color online) For $Ca_2Ru_{1-x}Mn_xO_4$ with $0 \leqslant x \leqslant 0.25$, x dependence of (a) the lattice parameters a, b, and c axes (right scale) at $T = 90$ K; (b) unit cell volume V; and (c) thermal expansion ratio $\Delta V/V$ ($= [V(295 \text{ K}) - V(90 \text{ K})]/V(295 \text{ K})$. Note that $\Delta V/V$ in (c) is only for 90 K $\leqslant T \leqslant$ 295 K, and this value is much greater for 90 K $\leqslant T \leqslant T_{MI} \sim$ 380 K.

FIG. 2. (Color online) For $Ca_2Ru_{1-x}Mn_xO_4$ with $x = 0.10$, temperature dependences of (a) lattice parameters a, b, and c axes (right scale); (b) unit cell volume V; and (c) magnetic susceptibility χ_{ab} at $\mu_o H = 0.5$ T (field cooled) and ab plane resistivity $\log_{10} \rho_{ab}$ (right scale). The shaded area indicates the concomitant occurrence of the NTE and MI transition.

Like Cr doping,[14,23] Mn doping preserves the low temperature orthorhombic symmetry (*Pbca*) but weakens the orthorhombic distortion by reducing the difference between the a and b axis or [b–a] from 0.25 Å for $x = 0$ to 0.07 Å for $x = 0.25$. Furthermore, the unit cell volume V for $x \geqslant 0.085$ is larger at 90 K than at 295 K, indication NTE; but the NTE diminishes when x approaches 0.25, as shown in Figs. 1(b) and 1(c).

We now focus on the coupling between the NTE and MI transition at T_{MI} and the magnetic order at T_N by examining two sets of representative data for $x = 0.10$ and 0.25. At $x = 0.10$, the NTE occurs along both the a and b axes; this combined effect results in an overall volume expansion ratio $\Delta V/V \approx 0.8\%$ on cooling with an onset in close proximity to the MI transition that occurs at $T_{MI} = 380$ K (ρ_{ab} is in $\log_{10}$ scale), as shown in Fig. 2. The coupling of the NTE to the MI transition and the magnetic order is obvious in that V rapidly expands below $T_{MI} = 380$ K and exhibits a weak yet well-defined anomaly near $T_N = 130$ K, where the weak ferromagnetic behavior takes place, as marked by the shaded area and the dashed line in Fig. 2. On the other hand, at $x = 0.25$, the orthorhombicity is considerably weakened and reduced to 225 K, and the MI transition becomes so broadened that it cannot be well defined. Concomitantly, the NTE diminishes with nearly zero thermal expansion, or $\Delta V/V$ <0.1%, when temperature is lowered from 410 K to 90 K, as illustrated in Fig. 3. The simultaneous disappearance of both
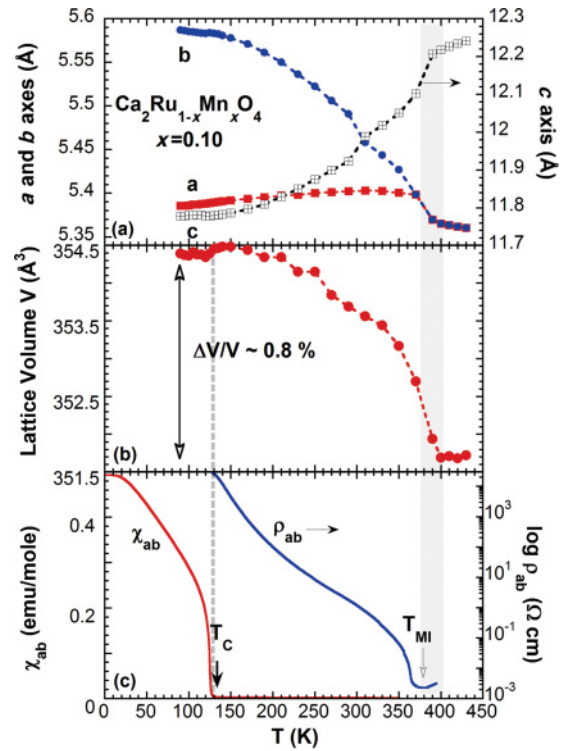
T_{MI} and the NTE reinforces that the NTE and the orbital order are indeed strongly coupled.

Figure 4 provides a comparison of the physical properties between several representative Mn concentrations. It is clear that the MI transition increases from $T_{MI} = 357$ K for $x = 0$ to ~380 K for $x = 0.085$ and 0.10, but the sharpness of the MI transition diminishes for $x = 0.14$ and vanishes for $x = 0.25$ [see Fig. 4(a)]. Since the MI transition is primarily due to the structural phase transition between the high-T tetragonal to the low-T orthorhombic distortion, the broadening of the MI transition is more likely due to the diminishing of the structural phase transition as Mn doping readily reduces the difference between the a and b axes, evident in Fig. 1(a). It needs to be pointed out that the MI transition in $Ca_2Ru_{1-x}Mn_xO_4$ is the second-order transition; this is in contrast to the first-order transition that characterizes Ca_2RuO_4[2,3] and $Ca_2Ru_{1-x}Cr_xO_4$.[14,23] The second-order phase transition at T_{MI} for various x is also confirmed by sharp peaks in specific heat $C(T)$, which are narrowly separated, as shown in Fig. 4(b). On the other hand, the magnetic ordering temperature T_N systematically rises with increasing x from $T_N = 120$ K for $x = 0.085$ to 130 K for $x = 0.10$ and eventually 150 K for $x = 0.25$, as illustrated in the inset in Fig. 4(b) and Fig. 4(c). (The systematic change of T_N with x further confirms the homogeneity of the samples studied.) Interestingly, Mn doping induces a metamagnetic transition at H_C and a sizable order moment μ_o; with increasing x, H_C decreases from 5 T for $x = 0.08$ to 2 T for $x = 0.25$,
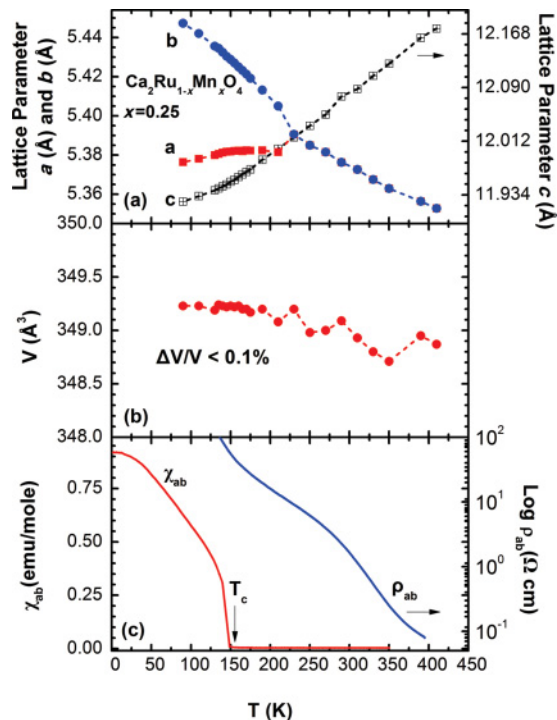
FIG. 3. (Color online) For $Ca_2Ru_{1-x}Mn_xO_4$ with $x = 0.25$, temperature dependences of (a) lattice parameters a, b, and c axes (right scale); (b) unit cell volume V; and (c) the magnetic susceptibility χ_{ab} at $\mu_o H = 0.05$ T and the ab plane resistivity ρ_{ab} (right scale).

whereas μ_o eventually amounts up to 0.2 μ_B/f.u. for $x = 0.25$, as shown in Fig. 4(d). The metamagnetism indicates a spin canting existent in an antiferromagnetic background, which explains the weak ferromagnetic behavior seen in Fig. 4(c).

B. $Ca_2Ru_{1-x}Fe_xO_4$ with $0 < x \leqslant 0.22$

Substituting Fe for Ru in Ca_2RuO_4 also effectively weakens the orthorhombic distortion and induces the NTE. Figure 5 registers the lattice parameters for $0.08 \leqslant x \leqslant 0.22$ taken at 90 K and 295 K. Similar to that for Cr[14,23] and Mn doping (Figs. 1 and 3), the effect of the NTE nearly vanishes at $x = 0.22$ where the orthorhombic distortion is considerably reduced and T_{MI} is no longer well defined.

More detailed data for $x = 0.08$ as a function of temperature collected over $1.7 < T < 450$ K exhibit the strong NTE along the b axis but a much weaker temperature dependence of the a axis [see Fig. 6(a)] and an overall thermal expansion with $\Delta V/V \sim 0.8\%$ on cooling over $90 < T < 390$ K [see Fig. 6(b)]. It is now no longer a surprise that the onset of the NTE occurs simultaneously with the MI transition at T_{MI} that is characterized by a strong anomaly in the specific heat $C(T)$ [Fig. 6(b)] and $\rho_{ab}(T)$ [Fig. 6(c), right scale] at $T_{MI} = 380$ K. It is noted that the NTE peaks near 150 K below which V starts to contract on cooling [Fig. 6(b)] and there is no obvious lattice anomaly near the magnetic order at $T_N = 120$ K, in contrast to the behavior seen in Cr- and Mn-doped Ca_2RuO_4. This difference may be associated with unusual magnetic properties absent in Cr- and Mn-doped Ca_2RuO_4. As seen in Fig. 6(c), χ_{ab} for $x = 0.08$ shows a peak at T_N seldom seen in other anti-
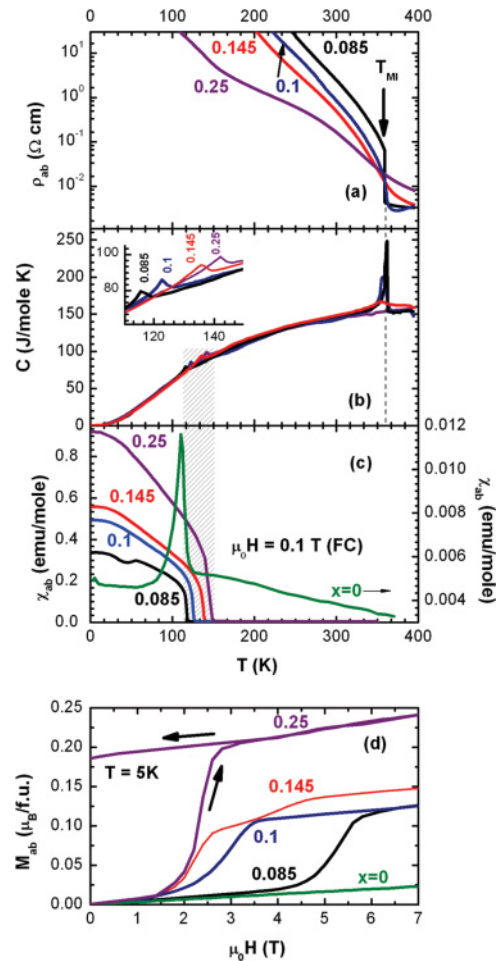

FIG. 4. (Color online) For $Ca_2Ru_{1-x}Mn_xO_4$ with $0 \leqslant x \leqslant 0.25$, temperature dependence of (a) the ab plane resistivity ρ_{ab}; (b) the specific heat $C(T)$; (c) magnetic suscepitibilty χ_{ab}; and (d) the isotheraml magnetization M_{ab}. Inset: enlarged $C(T)$ near T_N. Note that T_N and the order moment increase with x.

ferromagnets; this behavior is then evolved into "diamagnetic" behavior for $x = 0.12$ below $T_N = 120$ K, indicating a rare magnetization reversal [Fig. 6(c)] (χ_{ab} was measured using a field-cooled sequence; the magnetization reversal exists in $0.08 < x < 0.22$). A magnetization reversal is highly unusual but is not without precedent; it has been observed in a few ferromagnetic spinels and $Sr_3Ir_2O_7$.[27] It is conceivable that increasing Fe doping for Ru may lead to two inequivalent magnetic sublattices that are antiferromagnetically coupled; the magnetization reversal could be a result of different temperature dependences of the two individual magnetic sublattices. Without apparent spin canting, the magnetoelastic effect may not be strong enough to cause any additional lattice anomaly that features Cr- and Mn-doped Ca_2RuO_4.

C. General trends in $Ca_2Ru_{1-x}M_xO_4$

Substituting Ru with a 3d ion always induces a modest and yet critical NTE along the a axis, as shown in Fig. 7(a). It is this critical change that leads to a rather sizable thermal expansion ratio $\Delta V/V$ on cooling in $Ca_2Ru_{1-x}M_xO_4$. The fact that this phenomenon does not occur for $x = 0$ despite the strong effect

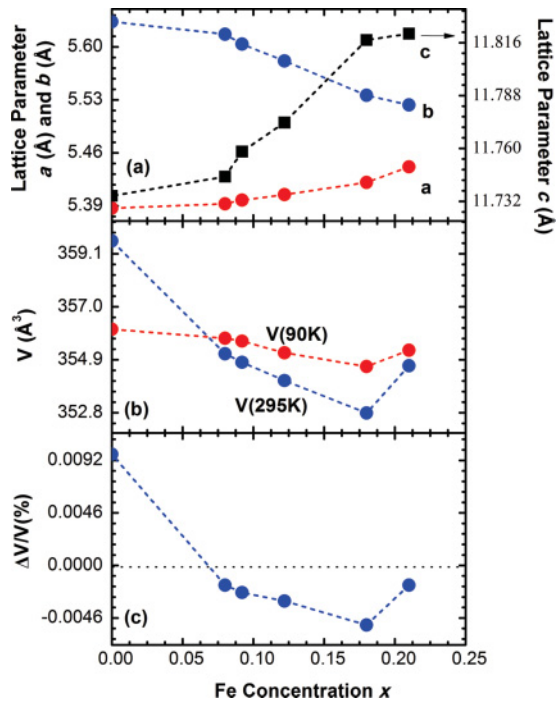FIG. 5. (Color online) For $Ca_2Ru_{1-x}Fe_xO_4$ with $0 \leqslant x \leqslant 0.22$, x dependence of (a) the lattice parameters a, b, and c axes (right scale) at $T = 90$ K; (b) unit cell volume V at $T = 90$ K and 295 K; and (c) thermal expansion ratio $\Delta V/V$ ($= [V(295$ K$) - V(90$ K$)]/V(295$ K$)$ for $0 \leqslant x \leqslant 0.22$.

of the NTE along the b axis underscores how critically M doping "unlocks" strongly buckled Ru/MO$_6$ octahedra and changes the t_{2g} orbital configuration in the basal plane. Indeed, the basal plane Ru/M-O1-Ru/M bond angle θ drastically decreases below T_{MI} that in turn simultaneously prompts an expansion of the Ru/M-O1 bond length d and the Ru/M-Ru/M distance on cooling, as shown in Figs. 7(b) and 7(c) for a representative compound $Ca_2Ru_{1-x}Fe_xO_4$ with $x = 0.08$, respectively. The expansion of d clearly outweighs positive thermal expansion due to longitudinal vibrational modes, allowing both the a and b axes to expand with cooling while preserving the structural symmetry; and as a result, V rapidly expands on cooling near T_{MI} where the t_{2g} orbital order takes place. Both the NTE and the orbital order in $Ca_2Ru_{1-x}M_xO_4$ closely track the changing orthorhombicity as x changes and disappear when the orthorhombicity vanishes near x_c, a critical doping concentration ($x_c = 0.14$, 0.25, 0.22, and 0.20 for Cr, Mn, Fe, and Cu, respectively). As for the magnetic state and the spin-lattice effect, it is recognized that an increase in the Ru-O2 bond length along the c axis destabilizes the collinear antiferromagnetic state,[28] resulting in strongly competing antiferromagnetic and ferromagnetic exchange interactions or spin canting below T_N in doped Ca_2RuO_4. Except for Fe doping, which does not seem to cause spin canting, the spin-lattice coupling or magnetoelastic effect is strong enough to generate an additional lattice anomaly near T_N. It is also noted that the magnitude of the NTE decreases as the atomic number of M increases. This interesting trend may be associated with the fact that with increasing nuclear charge the 3d orbitals become more contracted, and the 3d band progressively fills and
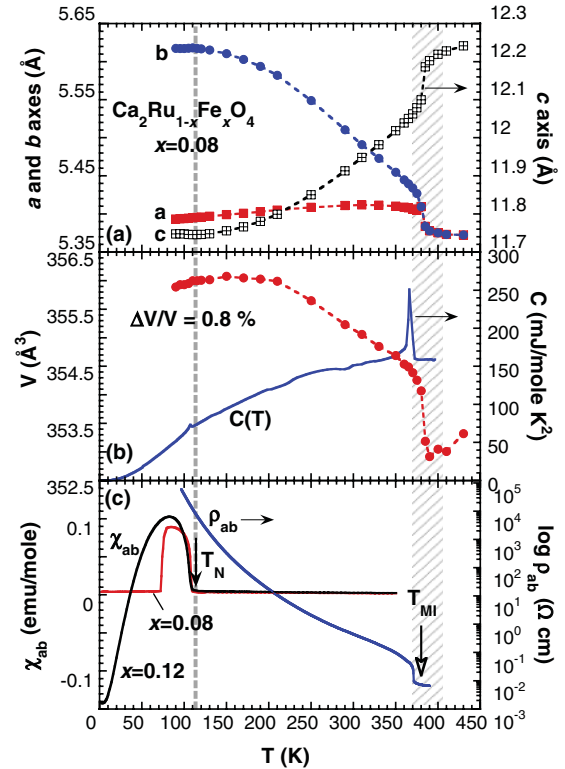

FIG. 6. (Color online) For $Ca_2Ru_{1-x}Fe_xO_4$ with $x = 0.08$, temperature dependences of (a) lattice parameters a, b, and c axes (right scale); (b) lattice volume V and specific heat $C(T)$ (right scale); and (c) magnetic susceptibility χ_{ab} at $\mu_0 H = 0.5$ T (field cooled) for both $x = 0.08$ and 0.12, as indicated, and ab plane resistivity $\log_{10} \rho_{ab}$ (right scale). Note the unusual magnetization reversal for $x = 0.12$.
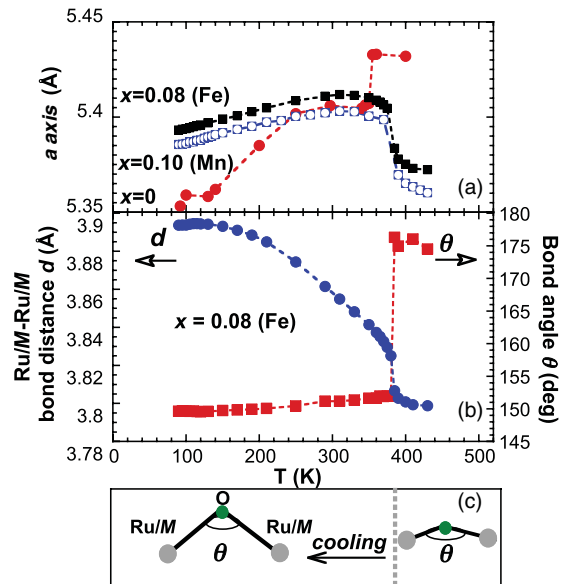

FIG. 7. (Color online) Temperature dependences of (a) lattice parameter a axis for $x = 0$, 0.10 (Mn) and 0.08 (Fe); (b) the Ru/M-Ru/M bond length d and the Ru/M-O1-Ru/M bond angle θ (right scale) for $x = 0.08$ (Fe); and (c) schematics illustrating changes of d and θ on cooling.

downshifts away from the Fermi energy E_F, thus weakening the overlapping with 4d band that stays near E_F.

It is compelling to attribute the observed NTE to a mechanism where electronic correlations play a critical role. Such a mechanism can be qualitatively discussed as follows. In a Mott insulator the occurrence of an orbital or magnetic order is always accompanied by electron localization. The electron localization costs kinetic energy of electrons whereas lattice expansion reduces the kinetic energy. Meanwhile, the lattice expansion costs the energy for electron-lattice interaction. Spin-lattice coupling also plays an important role in releasing frustration via phase transition; such a magnetovolume effect is significant when there is a strong competition between ferromagnetic and antiferromagnetic coupling, which often leads to strong bond frustration or lattice anomaly.[21] Indeed, NTE could happen if the energy gain from the electron-electron interaction and the lattice expansion can overcome the energy cost from the electron-lattice interaction and the electron localization. When the orbital and/or magnetic order takes place, the energy gain of electrons can be described in terms of the short range coupling parameters between orbital or spin orders; namely, if we use a local exchange effective model to describe the orbital or magnetic order,

$$H = \sum_{\langle ij \rangle} J_{ij} A_i A_j,$$

where A_j represents local spin or orbital moments. The effective coupling parameters J_{ij} are generally determined by virtual hopping processes. Therefore, if the lattice expansion increases J_{ij}, the orbital and/or magnetic order can make the NTE more energetically favorable; this is more likely in a multiorbital system where the Coulomb repulsion U is relatively small for the following reasons: (1) virtual hopping becomes much more complicated in effective bands due to the mixture of different orbitals; and (2) spin-orbit coupling and crystal field effects, which are strongly affected by the lattice expansion, become comparable to U. $Ca_2Ru_{1-x}M_xO_4$ are multiorbital systems with comparable U and spin-orbit interaction; therefore, the NTE happens but in a fashion fundamentally different from that of classic NTE materials, as shown in Figs. 1–7. A computational result on the values of J_{ij} following the previous analysis will be reported elsewhere.[29] This paper presents convincing evidence that the strong coupling of the NTE to the underlying physical properties exists in a class of the Mott insulators, doped Ca_2RuO_4, highlighting the new physics yet to be fully understood.

*cao@uky.edu

[1] Y. Meano, H. Hashimoto, K. Yoshida, S. Nishizaki, T. Fujita, J. G. Bednorz, and F. Lichtenberg, Nature **372**, 532 (1994).

[2] G. Cao, S. McCall, M. Shepard, J. E. Crow, and R. P. Guertin, Phys. Rev. B **56**, R2916 (1997).

[3] C. S. Alexander, G. Cao, V. Dobrosavljevic, S. McCall, J. E. Crow, E. Lochner, and R. P. Guertin, Phys. Rev. B **60**, R8422 (1999).

[4] M. Braden, G. Andre, S. Nakatsuji, and Y. Maeno, Phys. Rev. B **58**, 847 (1998).

[5] J. H. Jung, Z. Fang, J. P. He, Y. Kaneko, Y. Okimoto, and Y. Tokura, Phys. Rev. Lett. **91**, 056403 (2003).

[6] G.-Q. Liu, Phys. Rev. B **84**, 235136 (2011).

[7] C. S. Snow, S. L. Cooper, G. Cao, J. E. Crow, H. Fukazawa, S. Nakatsuji, and Y. Maeno, Phys. Rev. Lett. **89**, 226401 (2002).

[8] T. Hotta and E. Dagotto, Phys. Rev. Lett. **88**, 077202 (2001).

[9] T. Mizokawa, L. H. Tjeng, G. A. Sawatzky, G. Ghiringhelli, O. Tjernberg, N. B. Brookes, H. Fukazawa, S. Nakatsuji, and Y. Maeno, Phys. Rev. Lett. **87**, 077202 (2001).

[10] G. Cao, S. McCall, J. E. Crow, and R. P. Guertin, Phys. Rev. Lett. **78**, 1751 (1997).

[11] G. Cao, S. McCall, V. Dobrosavljevic, C. S. Alexander, J. E. Crow, and R. P. Guertin, Phys. Rev. B **61**, R5053 (2000).

[12] S. Nakatsuji and Y. Maeno, Phys. Rev. Lett. **84**, 2666 (2000).

[13] J. S. Lee, Y. S. Lee, T. W. Noh, S.-J. Oh, Jaejun Yu, S. Nakatsuji, H. Fukazawa, and Y. Maeno, Phys. Rev. Lett. **89**, 257402 (2002).

[14] T. F. Qi, O. B. Korneta, S. Parkin, L. E. De Long, P. Schlottmann, and G. Cao, Phys. Rev. Lett. **105**, 177203 (2010).

[15] T. A. Mary, J. S. O. Evans, T. Vogt, and A. W. Sleight, Science **272**, 90 (1996).

[16] J. R. Salvador, F. Guo, T. Hogan, and M. G. Kanatzidis, Nature **425**, 702 (2003).

[17] R. Lakes, Appl. Phys. Lett. **90**, 221905 (2007).

[18] A. L. Goodwin, M. Calleja, M. J. Conterio, M. T. Dove, J. S. O. Evans, D. A. Keen, L. Peters, and M. G. Tucker, Science **319**, 794 (2008).

[19] J. S. O. Evans, T. A. Mary, and A. W. Sleight, J. Solid State Chem. **133**, 580 (1997).

[20] N. H. Fletcher, *The Chemical Physics of Ice* (Cambridge University Press, Cambridge, 1970).

[21] J. Hemberger, H.-A. Krug von Nidda, V. Tsurkan, and A. Loid, Phys. Rev. Lett. **98**, 147203 (2007).

[22] M. Azuma, W.-t. Chen, H. Seki, M. Czapski, S. Olga, K. Oka, M. Mizumaki, T. Watanuki, N. Ishimatsu, N. Kawamura, S. Ishiwata, M. G. Tucker, Y. Shimakawa1, and J. P. Attfield Msaski Azuma, Nature Communications **2**, 1361 (2011).

[23] T. F. Qi, M. Ge, O. B. Korneta, S. Parkin, L. E. DeLong, and G. Cao, J. Solid State Chem. **184**, 893 (2011).

[24] G. M. Sheldrick, Acta Crystallogr. A **64**, 112 (2008).

[25] G. M. Sheldrick, *SADABS* (University of Göttingen, Germany, 1996).

[26] T. F. Qi and G. Cao (private communications, 2012).

[27] G. Cao, Y. Xin, C. S. Alexander, J. E. Crow, P. Schlottmann, M. K. Crawford, R. L. Harlow, and W. Marshall, Phys. Rev. B **66** 214412 (2002).

[28] Z. Fang and K. Terakura, Phys. Rev. B **64**, 020509 (2001).

[29] J. Hu (private communications, 2011).